

The role of anharmonicity in single-molecule spin-crossover

Chuan Guan and Yun-An Yan*

*School of Physics and Optoelectronic Engineering,
Ludong University, Yantai, Shandong 264025, China*

We exploit the system-bath paradigm to investigate vibrational-anharmonicity effects on spin-crossover in a single molecule. Focusing on weak coupling, we use the linear response approximation to deal with the nonlinear vibrational bath and propagate the Redfield master equation to obtain the equilibrium high spin fraction. We take both the anharmonicity in the bath potentials and the nonlinearity in the spin-vibration coupling into account and find a strong interplay between these two effects. Further, we show that the spin-crossover in a single molecule is always a gradual transition and the anharmonicity-induced phonon drag greatly affects the transition behavior.

* yunan@ldu.edu.cn

I. INTRODUCTION

Octahedral first-row transition-metal complexes of $3d^4$ - $3d^7$ may switch between the high-spin (HS) and the low-spin (LS) states under external perturbations, such as temperature change [1], light irradiation [2], pressure [3], magnetic field [4], and electric field [5]. Such a spin-crossover (SCO) [6–8] usually comes up with changes in magnetic moment, color [9], structure, dielectric constant [10], and even catalytic capacity [11]. Because of the rich physics and phenomena, SCO has wide potential applications in molecular switches [12], memory devices [13], sensors [14], actuators [15] and has aroused extensive research interests.

Among various SCO phenomena, the temperature-induced ones [16] are of special interest, in which energy splitting between the HS and the LS states are close to the thermal energy. In practical applications, the transition is required to be abrupt and occur at room temperature. In this case the vibrations will play a key role due to the energy matching [17, 18]. Various models have been proposed to understand the role of vibrations, including the Ising model extended with lattice vibration [19], the atom-phonon model [20], and the stretching-bending model [21].

Note that in metal-organic compounds, vibrations often assume strong anharmonicity due to the presence of hydrogen bonding or other intermolecular interactions. Shelest studied the thermodynamics of SCO with an anharmonic model and revealed that anharmonicity is one important parameter controlling the SCO transition [22]. Nicolazzi *et al.* used the Lennard-Jones potential to model intermolecular interactions and found that anharmonicity can reduce the transition temperature and make the HS state more stable [23–25]. These authors further demonstrated that anharmonicity in intermolecular interactions is pivotal to understand SCO in nanostructures which allows atoms to undergo large displacements away from their equilibrium positions [26]. Boukheddaden proposed an anharmonic coupling model and showed that change in anharmonicity drastically alters the SCO transition [27]. However, there are controversial conclusions in the literature. For instance, Wu *et al.* performed density functional theory calculations for the effects of anharmonicity on the zero-point energy and the entropy in Fe(II) and Fe(III) complexes and found a rather small contribution to SCO [28].

Besides in metal-organic compounds, anharmonicity exists in a wide variety of systems and has been attracting increasing research interests. Even though suppressed in crys-

tals by the crystal symmetry, lattice anharmonicity can still significantly affect crystal's kinetics, dynamics, and thermodynamics [29, 30]. This issue becomes more profound on surfaces [31] or in disordered systems, including polar liquids [32], glasses [33], and molecular systems [34, 35]. For example, Lunghi and coworkers found that the anharmonicity in single molecule magnets is responsible for fast under-barrier spin relaxation [36]. Now the anharmonicity-induced nonlinear effects and the underlying origin can be accessed with linear and ultrafast IR and Raman spectroscopies thanks to their tremendous progress in the past three decades [37–43].

When dealing with anharmonicity, available studies were based on either a classical description or the noninteracting, independent quantum oscillator model. Here we suggest a consistent quantum approach by using nonlinear quantum dissipation. In order to obtain a clear picture of the anharmonic effect itself and to avoid discussing complicated interplays between anharmonicity, spin pairing, energy splitting, and interactions among transition-metal centers, we focus on the single-molecule SCO transition in the weak spin-vibration coupling regime. A numerically exact simulation of an intrinsic nonlinear dissipation system is expensive. For the weak dissipation under study, we can approximate the bath with the anharmonic influence functional approach suggested by Makri *et al.* [44–46]. Eventually, the anharmonic influence functional approach maps the anharmonic bath to a harmonic one with the help of an effective spectral density function. After doing so, we can follow the quantum master equation (QME) approach developed for the linear dissipation to investigate single-molecule SCO. Note that simulations of SCO with QME was recently used by Orlov *et al.* [47, 48].

At first glance the use of a nonlinear bath model is *ad hoc* because the bath is always linear in the open system paradigm at any given temperature. Note that the dissipation theory is a phenomenological description of open systems based on the quantum fluctuation-dissipation theorem [49, 50]. One of the key points is the system-bath separation which implies that the system-bath interaction is weak and the effect of a single bath mode on the system is negligibly small. The effect of the bath, therefore, is a collective behavior and the system only feels the overall environmental fluctuation that follows the Gaussian statistics. The fluctuation of the bath is characterized by its spectral density function and can be reproduced with the linear-dissipation Caldeira-Leggett model [51]. This framework, however, only holds at a fixed temperature and in principle the spectral density functions at different

temperatures are not the same. In reality, all baths, especially for low-dimensional and molecular systems, are intrinsically anharmonic. The use of linear dissipation for simulating physics of an anharmonic system will have to adopt a different spectral density function, hence a different bath, for each temperature and therefore loses the predictive power for any temperature-dependent behavior. A remedy is the above-mentioned nonlinear dissipation model, in which the same bath is used to consistently yield the effective spectral density functions for all temperatures.

The rest of the paper are organized as follows. In Sec. II, we outline the anharmonic influence functional method in the linear response regime. In Sec. III, we present calculations with different anharmonic settings to check their effects on SCO. A concise summary and outlook are provided in Sec. IV.

II. THEORETICAL MODEL

We only investigate the one-step SCO transition which is dictated by the Hamiltonian

$$\hat{H}_{tot} = \begin{pmatrix} \epsilon_L + \hat{H}_{vib}^{(L)} & -\frac{\lambda}{2} \\ -\frac{\lambda}{2} & \epsilon_H + \hat{H}_{vib}^{(H)} \end{pmatrix}, \quad (1)$$

where λ is the spin-orbital coupling, ϵ_S are the electronic energy, and $\hat{H}_{vib}^{(S)}$ with $S = L$ and H describe the vibrations of the LS and the HS states, respectively. Here we discuss the anharmonic effects without considering the Duschinsky rotation and mode-mode coupling. Furthermore, we assume that the LS and the HS states have the same anharmonicity. With these approximations and up to the fourth order, the vibrational Hamiltonians can be extracted from separate, *ab initio* anharmonic force constant calculations at the LS and the HS states [52], yielding $\hat{H}_{vib}^{(S)} = \sum_j \left\{ \frac{\hat{p}_j^2}{2m_j} + v_{j,1}^{(S)} \hat{x}_j + v_{j,2}^{(S)} \hat{x}_j^2 + v_{j,3}^{(S)} \hat{x}_j^3 + v_{j,4}^{(S)} \hat{x}_j^4 \right\}$ with $v_{j,3}^{(L)} = v_{j,3}^{(H)}$ and $v_{j,4}^{(L)} = v_{j,4}^{(H)}$.

The Hamiltonian in Eq. (1) can be re-expressed in terms of the system-plus-bath model

$$\hat{H}_{tot} = \hat{H}_s + \hat{H}_b + \hat{H}_{sb}. \quad (2)$$

Here we set the Planck constant \hbar and the Boltzmann constant k_B to unity. The Hamiltonian for a two-state system in Eq. (2) can be represented as $\hat{H}_s = -\frac{\Delta}{2}\sigma_z - \frac{\lambda}{2}\sigma_x$, where $\Delta = \epsilon_H - \epsilon_L$ is the energy bias between the LS and the HS states and σ_z/σ_x are the spin-1/2 Pauli

matrices. Meanwhile, the Hamiltonian for the thermal bath is given by $\hat{H}_b = \sum_j [\hat{p}_j^2/(2m_j) + V_j(\hat{x}_j)]$, where $V_j(\hat{x}_j) = \frac{1}{2}m_j\omega_j^2\hat{x}_j^2(1 + b_j\sqrt{\omega_j}\hat{x}_j + a_j\omega_j\hat{x}_j^2)$ is the potential of the thermal bath, with a_j and b_j being coefficients characterizing bath anharmonicity. The Hamiltonian for the system-bath interaction is $\hat{H}_{sb} = \sigma_z \sum_j c_j(\hat{o}_j - \langle \hat{o}_j \rangle)$, where c_j denotes the coupling constant between the system and the environment, the operator $\hat{o}_j = \hat{x}_j + \kappa_j\sqrt{\omega_j}\hat{x}_j^2$ with κ_j being the nonlinear strength in the spin-vibration coupling, and $\langle \hat{o}_j \rangle = \text{Tr}[\hat{o}_j e^{-\beta\hat{H}_b}]/\text{Tr}e^{-\beta\hat{H}_b}$ denotes the equilibrium expectation of the operator \hat{o}_j .

Utilizing the linear response approximation, the effect of the bath is encapsulated by its correlation function [44–46]

$$\alpha(t) = \frac{1}{\pi} \int_0^\infty d\omega J_\beta(\omega) [\coth(\frac{\beta\omega}{2}) \cos \omega t - i \sin \omega t], \quad (3)$$

where $\beta = 1/T$ with T being the temperature, and $J_\beta(\omega)$ is the effective spectral density function

$$J_\beta(\omega) = \sum_{j,m,n} \frac{c_j^2 \pi}{4Z_j} (e^{-\beta\epsilon_n^{(j)}} - e^{-\beta\epsilon_m^{(j)}}) |o_{m,n}^{(j)}|^2 \delta(\omega - \omega_{mn}^{(j)}). \quad (4)$$

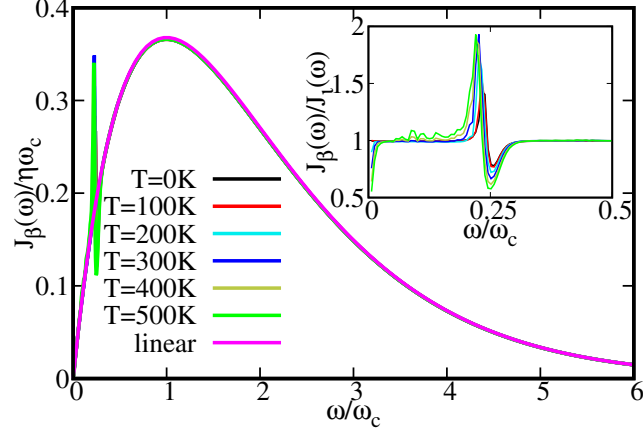
Here j is the index of the bath mode, $\epsilon_n^{(j)}$ denotes the n th eigen-energy, Z_j represents the partition function, and $\omega_{mn}^{(j)}$ stands for the transition frequency for $m \rightarrow n$. In the weak spin-vibration coupling regime under investigation, the Redfield equation can be used to obtain the equilibrium expectation

$$\frac{d\hat{\rho}(t)}{dt} = i[\hat{\rho}(t), \hat{H}_s] - [\sigma_z, (\hat{\Xi}\hat{\rho}(t) - \hat{\rho}(t)\hat{\Xi}^\dagger)], \quad (5)$$

where the operator $\hat{\Xi}$ is defined as

$$\hat{\Xi} = \int_0^\infty d\tau \alpha(\tau) e^{-i\hat{H}_s\tau} \sigma_z e^{i\hat{H}_s\tau}. \quad (6)$$

Equation (5) is the working equation of this work. Some remarks are in order. First, Eq. (5) and the underlying system-bath paradigm are based on the assumption of a weak spin-vibration coupling. A natural question arises: How weak is weak enough to be handled with the above scheme? The answer depends on specific systems. Here we discuss this issue with a specific setting mimicking the typical temperature-induced SCO, *i.e.*, $\Delta = \lambda = 50$ meV, $T < 300$ K, and with a high-frequency cutoff of 800 cm^{-1} for the heat bath. Analog to the linear dissipation, we adopt the renormalization energy $E_r = \int_0^\infty d\omega J_\beta(\omega)/\omega$



"0.00-0.24.dat" u (\$1*
 "0.20-0.24.dat" u (\$1*
 "0.40-0.24.dat" u (\$1*
 "0.60-0.24.dat" u (\$1*
 "0.80-0.24.dat" u (\$1*
 "1.00-0.24.dat" u (\$1*

FIG. 1. Effective spectral density function at different temperatures. The parameters in the nonlinear dissipation part are $a_j = 0.0043253\omega_j^3/((15 + \omega_j)(1 - 31.52\omega_j^2 + 256\omega_j^4)^2)$, $b_j = -0.49020\omega_j^{3/2}/((15 + \omega_j)(1 - 31.52\omega_j^2 + 256\omega_j^4))$, and $\kappa_j = 0$. The parameters c_j and ω_j for the linear part is determined by discretizing the spectral density $J_l(\omega) = 0.05\omega \exp(-\omega/\omega_c)$ with 20 000 modes. Check text for details about the Hamiltonian.

to characterize the overall coupling strength. Model simulations show that in the absence of anharmonicity, calculations with $E_r = 25$ meV can produce reliable results. In the presence of significant anharmonicity, we should be more cautious and limit the dissipation strength up to 10 meV.

In realistic SCO systems the spin-vibration coupling is not necessarily weak. For instance, in the two-dimensional layer $[\text{Fe}^{\text{II}}((3,5\text{-}(\text{CH}_3)_2\text{Pz})_3\text{BH})_2]$ (Pz = pyrazolyl), the spin-vibration coupling constants of one or two modes lie between 20 meV and 50 meV and the rest are below 10 meV [53]. Such a separation that the spin-vibration coupling is dominated by one or two particular modes is not unique for $[\text{Fe}^{\text{II}}((3,5\text{-}(\text{CH}_3)_2\text{Pz})_3\text{BH})_2]$ but widely exists in many SCO complexes [54, 55]. In this case we can follow the treatments adopted in the context of exciton dynamics to include these modes into the system and treat the rest modes as a heat bath [56]. The remaining spin-vibration coupling then becomes sufficiently weak to allow a QME treatment. The above procedure is therefore applicable with a direct enlargement of the system.

Second, beyond the weak coupling regime, a universal nonlinear-dissipation theory is yet to be developed but methods are available for specific cases. For systems that can be reasonably modeled with the lowest-level nonlinearity (harmonic potentials with linear

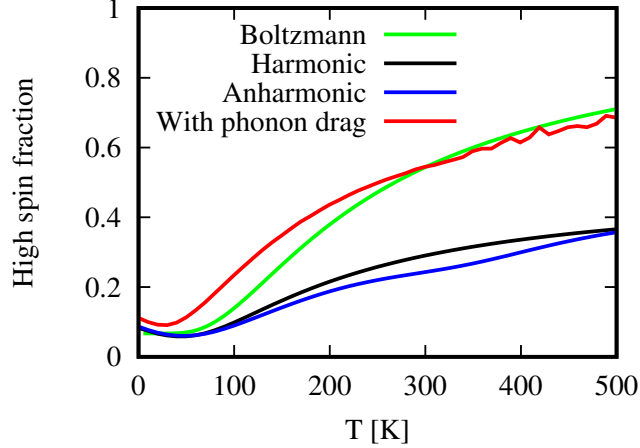


FIG. 2. The effects of the anharmonicity in the bath potential on SCO. Boltzmann: Results given by the Boltzmann distribution; Harmonic: Equilibrium results of the Redfield equation with $a_j = 0$, $b_j = 0$, and $\kappa_j = 0$; Anharmonic: Equilibrium results with anharmonicity in the bath potential only; With phonon drag: The thermal average $\langle \hat{o}_j \rangle$ is included in energy splitting. Parameters κ_j , a_j , and b_j for the latter two are the same as that in Fig. 1.

plus quadratic spin-vibration couplings), more advanced methods, such as the hierarchical equation of motion [57] and the quantum stochastic Liouville equation [58] are useful to tackle the physics.

Third and the last, here we focus on transitions in a single molecule and therefore not include cooperative interactions between metal centers which are pivotal to implement practical SCO materials. However, the open system paradigm, as a generic framework to tackle quantum dissipative dynamics, can be straightforwardly extended to oligomers or lattices. To be specific, the Hamiltonian \hat{H}_{tot} can be generalized to a nonlinearly-dissipated quantum Ising model [59, 60], that is, $\hat{H}_s = \sum_a [\frac{\Delta_a}{2} \sigma_a^x + \frac{\epsilon_a}{2} \sigma_a^z] + \sum_{ab} K_{ab} \sigma_a^z \sigma_b^z$ and $\hat{H}_{sb} = \sum_a \sigma_a^z \sum_j c_{j,a} (\hat{o}_j - \langle \hat{o}_j \rangle)$. Here σ_a^z (σ_a^x), Δ_a , and ϵ_a denote the Pauli matrices, the energy bias, and the spin-orbital coupling on site a , respectively, $c_{j,a}$ stands for the coupling constant between the a th spin and the j th vibration, and K_{ab} refers to the nearest neighbor interaction along z -direction. In this model the cooperative effects are encoded in the effective direct spin-spin interaction K_{ab} and the coupling of different spins to the same vibrational modes. As illustrated by Wolny and coworkers [61, 62], the parameters can again be extracted from *ab initio* calculations.

III. NUMERICAL RESULTS AND DISCUSSIONS

Here we adopt a discretized description for the anharmonic bath [63]. To this end, we determine the parameters c_j and ω_j upon discretizing the spectral density function $J_\iota(\omega) = \eta\omega \exp(-\omega/\omega_c)$ with 20 000 modes, where η is the linear dissipation strength and ω_c is the high frequency cutoff. For the anharmonic coefficients, we set $a_j = \omega_c/(2\omega_j x_{j,-} x_{j,+})$, $b_j = -2\sqrt{\omega_c}(x_{j,-} + x_{j,+})/(3\sqrt{\omega_j} x_{j,-} x_{j,+})$, where $x_{j,\pm} = f(\omega_j/\omega_c)(1 \pm 0.2\sqrt{1 - 1.6\omega_j/\omega_c})$ with $f(u) = \alpha(8u^2 + 1/32u^2 + \gamma)$. Here α and γ are two parameters controlling anharmonicity. Under these conditions, the bath modes with $\omega_j < \omega_c/1.6$ assume a double-well potential.

In this study we set $\Delta = 300$ K, $\lambda = 50$ meV, $\eta = 0.05$, $\omega_c = 800$ cm⁻¹, $\alpha = 1360$, and $\gamma = -0.985$. The parameters κ_j will be set to the same value for all vibrations, varying from 0 to 0.05 in step of 0.01. The calculated correlation functions for temperatures from 0 K to 500 K with intervals of 10 K are substituted into the Redfield equation to obtain the equilibrium distributions.

In Fig. 1 we present the effective spectral density functions for temperatures from 0 K to 500 K in step of 100 K. In the simulations, we first calculate the bath correlation function and perform the Fourier transform of its imaginary part to obtain the effective spectral density functions. For comparison we also plot the ratio $J_\beta(\omega)/J_\iota(\omega)$. As illustrated in Fig. 1, we observe that the effective spectral density function becomes temperature-dependent and deviates from the linear one. The overwhelming feature is that a sharp peak appears around $\omega = 0.22\omega_c$ besides the original peak of the linear spectral density function. The anharmonic results merge to linear dissipation when $\omega > 0.4\omega_c$.

We now discuss the effect of the anharmonicity in the bath potentials without the nonlinearity in the spin-vibration coupling. The results with linear dissipation are also presented. As shown in Fig. 2, with the anharmonic model, the HS fraction first decreases and then gradually increases with temperature. Even at a temperature as high as 500 K, the HS fraction is still less than one half. The harmonic model assumes roughly the same trend as the anharmonic one. However, subtle differences exist between the two trends, mainly in the temperature range from 100 K to 300 K, which is exactly the region in which the effective spectral density function deviates from its linear counterpart. It seems that the presence of the anharmonicity in the bath potential alone slows down the LS to the HS transition. For comparison we show the results obtained from the Boltzmann distribution.

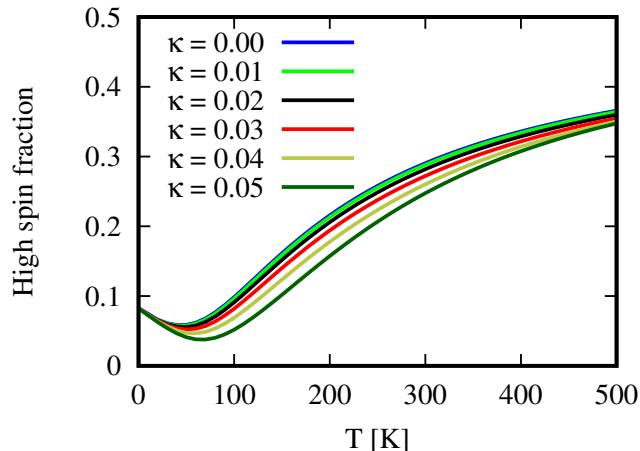


FIG. 3. The effects of nonlinear spin-vibration coupling with harmonic bath potential. The parameter κ_j are the same for all vibrations.

It is interesting to note that even for such a weak dissipation, the results from QME are significantly different from the Boltzmann distribution.

Next we investigate the effect of the nonlinearity in the spin-vibration coupling without the potential anharmonicity. The results are shown in Fig. 3, which depicts the same overall trend as that in Fig. 2. For different nonlinear intensities characterized with κ , the differences are pretty small and only obvious between 100 K and 300 K.

In the presence of both the anharmonicity in the bath potential and the nonlinearity in spin-vibration coupling, there may have strong interplay between these two effects. As shown in Fig. 4, now the temperature dependence are much more significant than that in Figs. 2 and 3, especially in the temperature range from 100 K to 300 K. With such an interplay, the HS fraction changes much abrupter with temperature for stronger nonlinear spin-vibration coupling.

The vibrational anharmonicity will affect SCO via another mechanism. When the system jumps between the HS and the LS states, the vibrational environment the spin feels is switched between $\hat{H}_{vib}^{(L)}$ and $\hat{H}_{vib}^{(H)}$ that are specified in Eq. (1). From the view point of reduced dynamics, the energy splitting between HS and LS is in principle $\Delta = \epsilon_H - \epsilon_L + \langle \hat{H}_{vib}^{(H)} - \hat{H}_{vib}^{(L)} \rangle$. The thermal equilibrium expectations $\langle \hat{H}_{vib}^{(S)} \rangle$ ($S = H, L$) differ for different spin states in the presence of potential anharmonicity, and the molecular structure will be distorted according to the spin change. This equilibrium shift, which is absent for harmonic baths,

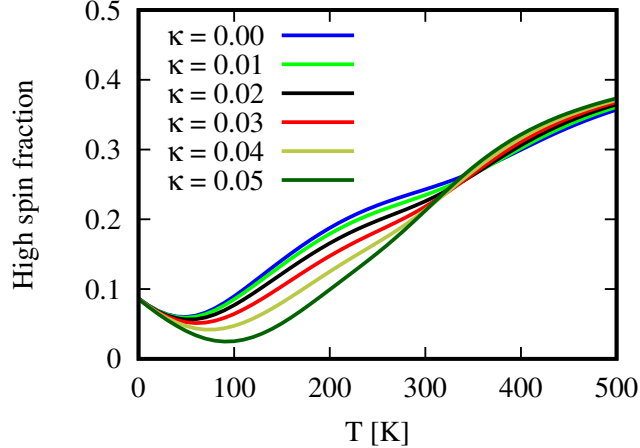


FIG. 4. The interplay of the nonlinearity in the spin-vibration coupling and the anharmonicity in the potential. Anharmonic parameters a_j and b_j are the same as that in Fig. 1.

introduces an additional energy splitting $\sum_j c_j \langle \hat{o}_j \rangle$ to SCO. Such a back-action mechanism of spin-induced molecular structure distortion is essentially the phonon drag effect observed in thermoelectric transportation [64–66]. However, there are subtle differences between these two cases. In thermoelectric transportation the phonon drag stems from the phonon motion against the temperature gradient and is mostly evidenced at low temperatures. In temperature-induced SCO the key role of drag effects is due to the temperature-dependent energy splitting reflecting the temperature-dependent distortion of the molecular structure. It is expected that the drag effects in SCO are manifested for temperatures under which the average molecular structures are significantly different between the HS and the LS configuration. To characterize this phonon drag effect, we set all c_j coefficients to positive in the bath discretization and add the thermal average $\sum_j c_j \langle \hat{o}_j \rangle$ to Δ . Note that in calculating the thermal average $\langle \hat{o}_j \rangle$, the quadratic term \hat{x}_j^2 always assumes a temperature-dependent result. In order to simplify the analysis and focus on the phonon drag effect we use $\kappa = 0$ to exclude the effect of nonlinear spin-vibration coupling. The corresponding results are demonstrated in Fig. 2, which shows that the phonon drag leads to a more pronounced and much abrupt temperature-dependence of the HS fraction.

IV. SUMMARY AND OUTLOOK

In metal-organic compounds, vibrations may assume strong anharmonicity. To take account of the anharmonicity effect on the temperature-induced SCO, a linear dissipation model has to adopt a separate spectral density function at each temperature and thus fails to describe the temperature-dependent transition. Here an anharmonic vibrational bath model is used to simulate single-molecule SCO. With the linear response approximation, we are able to obtain the effective spectral density functions for all temperatures consistently with the same bath that can be extracted from *ab initio* calculations. To scrutinize the anharmonicity effect itself, we focus on the weak spin-vibration coupling to avoid further complications caused by strong interaction. Propagating the Redfield equation to sufficiently long time, we can obtain the equilibrium distribution of the spin.

With specific double-well potentials for low-frequency vibrations, we have shown that the effective spectral density functions assume significant temperature dependency. We have performed four series of calculations with the obtained temperature-dependent spectral density functions: (1) anharmonicity in the bath potentials only; (2) nonlinearity in spin-vibration couplings only; (3) anharmonic bath potentials together with nonlinear spin-vibration couplings; (4) including the energy difference associated with the spin-induced molecular structure distortion. We have revealed that nonlinearities in the couplings or the potentials alone produce weak effects but their combination yields much stronger influence. Further, we have demonstrated that in the presence of anharmonicity, the SCO is drastically affected by the spin- and temperature-dependent thermal-average of vibrational degrees of freedom and becomes much abrupter. We have called it the phonon drag effect because it is essentially the same mechanism first found in thermoelectric transportation.

Here we only consider single-molecule transitions in the weak spin-vibration coupling regime. With the nonlinearly-dissipated quantum Ising model, our approach can be extended to study the cooperative effects in a molecular chain or lattice. Further, we can go beyond weak coupling assumption for those systems in which the spin-vibration interaction is dominated by one particular mode. Such a mode can be approximately included in QME as a two-level system because it is generally a breathing vibration and its second- and higher-excited states are only slightly populated at temperatures under 300 K. Then, with today's moderate computational resources, we can simulate the physics of a system up to 8

sites if this particular vibration is explicitly treated with QME and up to 16 sites otherwise. As such, we can have a consistent quantum description to scrutinize the interplay between anharmonicity, center-center cooperative interactions, and other factors.

ACKNOWLEDGMENTS

The authors acknowledge the support from the National Natural Science Foundation of China under grant No. 21973036.

-
- [1] P. Gütllich, A. Hauser, and H. Spiering, Thermal and optical switching of Iron(II) complexes, *Angew. Chem. Int. Ed.* **33**, 2024 (1994).
 - [2] A. Hauser, Reversibility of light-induced excited spin state trapping in the $\text{Fe}(\text{ptz})_6(\text{BF}_4)_2$, and the $\text{Zn}_{1-x}\text{Fe}_x(\text{ptz})_6(\text{BF}_4)_2$ spin-crossover systems, *Chem. Phys. Lett.* **124**, 543 (1986).
 - [3] G. Molnár, V. Niel, J.-A. Real, L. Dubrovinsky, A. Bousseksou, and J. J. McGarvey, Raman spectroscopic study of pressure effects on the spin-crossover coordination polymers $\text{Fe}(\text{Pyrazine})[\text{M}(\text{CN})_4] \cdot 2\text{H}_2\text{O}$ (M= Ni, Pd, Pt). First observation of a Piezo-Hysteresis loop at room temperature, *J. Phys. Chem. B* **107**, 3149 (2003).
 - [4] A. Bousseksou, K. Boukheddaden, M. Goiran, C. Consejo, M.-L. Boillot, and J.-P. Tuchagues, Dynamic response of the spin-crossover solid $\text{Co}(\text{H}_2(\text{fsa})_2\text{en})(\text{py})_2$ to a pulsed magnetic field, *Phys. Rev. B* **65**, 172412 (2002).
 - [5] F. Prins, M. Monrabal-Capilla, E. A. Osorio, E. Coronado, and H. S. J. van der Zant, Room-temperature electrical addressing of a bistable spin-crossover molecular system, *Adv. Mater.* **23**, 1545 (2011).
 - [6] L. Cambi and L. Szegö, Über die magnetische susceptibilität der komplexen verbindungen, *Ber. Dtsch. Chem. Ges. (A and B Ser.)* **64**, 2591 (1931).
 - [7] S. Brooker, Spin crossover with thermal hysteresis: Practicalities and lessons learnt, *Chem. Soc. Rev.* **44**, 2880 (2015).
 - [8] A. Bousseksou, G. Molnár, L. Salmon, and W. Nicolazzi, Molecular spin crossover phenomenon: Recent achievements and prospects, *Chem. Soc. Rev.* **40**, 3313 (2011).

- [9] O. Kahn, J. Kröber, and C. Jay, Spin transition molecular materials for displays and data recording, *Adv. Mater.* **4**, 718 (1992).
- [10] A. Bousseksou, G. Molnár, P. Demont, and J. Menegotto, Observation of a thermal hysteresis loop in the dielectric constant of spin crossover complexes: Towards molecular memory devices, *J. Mater. Chem.* **13**, 2069 (2003).
- [11] W. Zhong, Y. Liu, M. Deng, Y. Zhang, C. Jia, O. V. Prezhdo, J. Yuan, and J. Jiang, C₂N-supported single metal ion catalysts for HCOOH dehydrogenation, *J. Mater. Chem. A* **6**, 11105 (2018).
- [12] S. Bhandary, J. M. Tomczak, and A. Valli, Designing a mechanically driven spin-crossover molecular switch via organic embedding, *Nanoscale Adv.* **3**, 4990 (2021).
- [13] O. Kahn and C. J. Martinez, Spin-transition polymers: From molecular materials toward memory devices, *Science* **279**, 44 (1998).
- [14] J. Linares, E. Codjovi, and Y. Garcia, Pressure and temperature spin crossover sensors with optical detection, *Sensors* **12**, 4479 (2012).
- [15] G. Molnár, S. Rat, L. Salmon, W. Nicolazzi, and A. Bousseksou, Spin crossover nanomaterials: From fundamental concepts to devices, *Adv. Mater.* **30**, 1703862 (2018).
- [16] M. S. Shongwe, B. A. Al-Rashdi, H. Adams, M. J. Morris, M. Mikuriya, and G. R. Hearne, Thermally induced two-step, two-site incomplete ${}^6A_1 \leftrightarrow {}^2T_2$ crossover in a mononuclear Iron(III) phenolate-pyridyl Schiff-base complex: A rare crystallographic observation of the coexistence of pure $S=5/2$ and $1/2$ metal centers in the asymmetric unit, *Inorg. Chem.* **46**, 9558 (2007).
- [17] K. L. Ronayne, H. Paulsen, A. Höfer, A. C. Dennis, J. A. Wolny, A. I. Chumakov, V. Schünemann, H. Winkler, H. Spiering, A. Bousseksou, P. Gülich, A. X. Trautwein, and J. J. McGarvey, Vibrational spectrum of the spin crossover complex [Fe(phen)₂(NCS)₂] studied by IR and Raman spectroscopy, nuclear inelastic scattering and DFT calculations, *Phys. Chem. Chem. Phys.* **8**, 4685 (2006).
- [18] Y. Zhang, Predicting critical temperatures of Iron (II) spin crossover materials: Density functional theory plus U approach, *J. Chem. Phys.* **141**, 214703 (2014).
- [19] R. Zimmermann and E. König, A model for high-spin/low-spin transitions in solids including the effect of lattice vibrations, *J. Phys. Chem. Solids* **38**, 779 (1977).

- [20] J. A. Nasser, S. Topçu, L. Chassagne, M. Wakim, B. Bennali, J. Linares, and Y. Alayli, Two-dimensional atom-phonon coupling model for spin conversion: Role of metastable states, *Eur. Phys. J. B* **83**, 115 (2011).
- [21] H.-Z. Ye, C. Sun, and H. Jiang, Monte-Carlo simulations of spin-crossover phenomena based on a vibronic Ising-like model with realistic parameters, *Phys. Chem. Chem. Phys.* **17**, 6801 (2015).
- [22] V. V. Shelest, A. V. Khristov, and G. G. Levchenko, The role of anharmonicity in the systems with spin crossover, *Low Temp. Phys.* **42**, 505 (2016).
- [23] W. Nicolazzi, S. Pillet, and C. Lecomte, Two-variable anharmonic model for spin-crossover solids: A like-spin domains interpretation, *Phys. Rev. B* **78**, 174401 (2008).
- [24] W. Nicolazzi, J. Pavlik, S. Bedoui, G. Molnár, and A. Bousseksou, Elastic Ising-like model for the nucleation and domain formation in spin crossover molecular solids, *Eur. Phys. J. Spec. Top.* **222**, 1137 (2013).
- [25] M. Mikolasek, W. Nicolazzi, F. Terki, G. Molnár, and A. Bousseksou, Surface transition in spin crossover nanoparticles, *Chem. Phys. Lett.* **678**, 107 (2017).
- [26] A. Fahs, S. Mi, W. Nicolazzi, G. Molnár, and A. Bousseksou, Disentangling surface energy and surface/interface stress effects in spin crossover nanomaterials, *Adv. Phys. Res.* **2**, 2200055 (2023).
- [27] K. Boukheddaden, Anharmonic model for phonon-induced first-order transition in 1-D spin-crossover solids, *Prog. Theor. Phys.* **112**, 205 (2004).
- [28] J. Wu, C. Sousa, and C. de Graaf, The role of vibrational anharmonicity in the computational study of thermal spin crossover, *Magnetochemistry* **5**, 49 (2019).
- [29] R. A. Cowley, The lattice dynamics of an anharmonic crystal, *Adv. Phys.* **12**, 421 (1963).
- [30] M. E. Manley, O. Hellman, N. Shulumba, A. F. May, P. J. Stonaha, J. W. Lynn, V. O. Garlea, A. Alatas, R. P. Hermann, J. D. Budai, H. Wang, B. C. Sales, and A. J. Minnich, Intrinsic anharmonic localization in thermoelectric PbSe, *Nat. Commun.* **10**, 1928 (2019).
- [31] G. K. Wertheim, D. M. Riffe, and P. H. Citrin, Anharmonic surface vibrations in photoemission from alkali metals, *Phys. Rev. B* **49**, 2277 (1994).
- [32] G. R. Fleming and M. Cho, Chromophore-solvent dynamics, *Ann. Rev. Phys. Chem.* **47**, 109 (1996).

- [33] G. Baldi, V. M. Giordano, B. Ruta, R. Dal Maschio, A. Fontana, and G. Monaco, Anharmonic damping of terahertz acoustic waves in a network glass and its effect on the density of vibrational states, *Phys. Rev. Lett.* **112**, 125502 (2014).
- [34] Y.-A. Yan and O. Kühn, Unraveling the correlated dynamics of the double hydrogen bonds of nucleic acid base pairs in solution, *J. Phys. Chem. B* **115**, 5254 (2011).
- [35] A. Galestian Pour, C. N. Lincoln, V. Perlík, F. Šanda, and J. Hauer, Anharmonic vibrational effects in linear and two-dimensional electronic spectra, *Phys. Chem. Chem. Phys.* **19**, 24752 (2017).
- [36] A. Lunghi, F. Totti, R. Sessoli, and S. Sanvito, The role of anharmonic phonons in under-barrier spin relaxation of single molecule magnets, *Nat. Commun.* **8**, 14620 (2017).
- [37] S. A. Passino, Y. Nagasawa, and G. R. Fleming, Three pulse stimulated photon echo experiments as a probe of polar solvation dynamics: Utility of harmonic bath models, *J. Chem. Phys.* **107**, 6094 (1997).
- [38] T. Tayagaki and K. Tanaka, Photoinduced phase transition to a new macroscopic spin-crossover-complex phase, *Phys. Rev. Lett.* **86**, 2886 (2001).
- [39] K. Okumura, D. M. Jonas, and Y. Tanimura, Two-dimensional spectroscopy and harmonically coupled anharmonic oscillators, *Chem. Phys.* **266**, 237 (2001).
- [40] E. C. Fulmer, P. Mukherjee, A. T. Krummel, and M. T. Zanni, A pulse sequence for directly measuring the anharmonicities of coupled vibrations: Two-quantum two-dimensional infrared spectroscopy, *J. Chem. Phys.* **120**, 8067 (2004).
- [41] A. Ould-Hamouda, B. Viquerat, J. Degert, S. F. Matar, J. F. Létard, F. Guillaume, and E. Freysz, Impact of spin state transition on vibrations of $[\text{Fe}-(\text{PM-BiA})_2(\text{NCS})_2]$ and $[\text{Fe}-(\text{PM-PEA})_2(\text{NCS})_2]$ spin crossover compounds: Experimental and theoretical far IR and Raman study, *Eur. J. Inorg. Chem.* **2018**, 385 (2018).
- [42] K. B. Beć, J. Grabska, and Y. Ozaki, Advances in anharmonic methods and their applications to vibrational spectroscopies, in *Frontiers of Quantum Chemistry*, edited by M. J. Wójcik, H. Nakatsuji, B. Kirtman, and Y. Ozaki (Springer, Singapore, 2018) pp. 483–512.
- [43] Z. G. Lada, The investigation of spin-crossover systems by Raman spectroscopy: A review, *Magnetochemistry* **8**, 108 (2022).
- [44] G. Ilk and N. Makri, Real time path integral methods for a system coupled to an anharmonic bath, *J. Chem. Phys.* **101**, 6708 (1994).

- [45] N. Makri, The linear response approximation and its lowest order corrections: An influence functional approach, *J. Phys. Chem. B* **103**, 2823 (1999).
- [46] N. Makri, Iterative evaluation of the path integral for a system coupled to an anharmonic bath, *J. Chem. Phys.* **111**, 6164 (1999).
- [47] Y. S. Orlov, S. V. Nikolaev, A. I. Nesterov, and S. G. Ovchinnikov, Light-induced ultrafast dynamics of spin crossovers under high pressure, *J. Exp. Theor. Phys.* **132**, 399 (2021).
- [48] Y. S. Orlov, S. V. Nikolaev, and S. G. Ovchinnikov, Light-induced ultrafast dynamics of spin crossovers in LaCoO_3 , [arXiv: 2211.01300](#) (2022).
- [49] H. Mori, Transport, collective motion, and Brownian motion, *Prog. Theo. Phys.* **33**, 423 (1965).
- [50] R. Kubo, The fluctuation-dissipation theorem, *Rep. Prog. Phys.* **29**, 255 (1966).
- [51] A. O. Caldeira and A. J. Leggett, Influence of dissipation on quantum tunneling in macroscopic systems, *Phys. Rev. Lett.* **46**, 211 (1981).
- [52] K. Giese, M. Petković, H. Naundorf, and O. Kühn, Multidimensional quantum dynamics and infrared spectroscopy of hydrogen bonds, *Phys. Rep.* **430**, 211 (2006).
- [53] K. Bairagi, O. Iasco, A. Bellec, A. Kartsev, D. Li, J. Lagoute, C. Chacon, Y. Girard, S. Rousset, F. Miserque, Y. J. Dappe, A. Smogunov, C. Barreteau, M.-L. Boillot, T. Mallah, and V. Repain, Molecular-scale dynamics of light-induced spin cross-over in a two-dimensional layer, *Nat. Commun.* **7**, 12212 (2016).
- [54] H. T. Lemke, K. S. Kjær, R. Hartsock, T. B. van Driel, M. Chollet, J. M. Glowia, S. Song, D. Zhu, E. Pace, S. F. Matar, M. M. Nielsen, M. Benfatto, K. J. Gaffney, E. Collet, and M. Cammarata, Coherent structural trapping through wave packet dispersion during photoinduced spin state switching, *Nat. Commun.* **8**, 15342 (2017).
- [55] E. Svensson Grape, A. M. Davenport, and C. K. Brozek, Dynamic metal-linker bonds in metal—organic frameworks, *Dalton Trans.* **53**, 1935 (2024).
- [56] O. Kühn, T. Renger, and V. May, Theory of exciton-vibrational dynamics in molecular dimers, *Chem. Phys.* **204**, 99 (1996).
- [57] R. X. Xu, Y. Liu, H. Zhang, and Y. J. Yan, Theories of quantum dissipation and nonlinear coupling bath descriptors, *J. Chem. Phys.* **148**, 114103 (2018).
- [58] Y.-A. Yan, Stochastic simulation of anharmonic dissipation. II. Harmonic bath potentials with quadratic couplings, *J. Chem. Phys.* **150**, 074106 (2019).

- [59] J. Jin, A. Biella, O. Viyuela, C. Ciuti, R. Fazio, and D. Rossini, Phase diagram of the dissipative quantum Ising model on a square lattice, *Phys. Rev. B* **98**, 241108(R) (2018).
- [60] K. Le Hur, L. Henriot, L. Herviou, K. Plekhanov, A. Petrescu, T. Goren, M. Schiro, C. Mora, and P. P. Orth, Driven dissipative dynamics and topology of quantum impurity systems, *C. R. Phys.* **19**, 451 (2018).
- [61] S. Rackwitz, W. Klopper, V. Schünemann, and J. A. Wolny, Quantification of intramolecular cooperativity in polynuclear spin crossover Fe(II) complexes by density functional theory calculations, *Phys. Chem. Chem. Phys.* **15**, 15450 (2013).
- [62] J. A. Wolny, I. Faus, J. Marx, R. Ruffer, A. I. Chumakov, K. Schlage, H. Wille, and V. Schünemann, Vibrational coupling of nearest neighbors in 1-D spin crossover polymers of rigid bridging ligands. A nuclear inelastic scattering and DFT study, *Magnetochemistry* **2**, 19 (2016).
- [63] H. Wang and M. Thoss, Quantum dynamical simulation of electron-transfer reactions in an anharmonic environment, *J. Phys. Chem. A* **111**, 10369 (2007).
- [64] H. P. R. Frederikse, Thermoelectric power of germanium below room temperature, *Phys. Rev.* **92**, 248 (1953).
- [65] C. Herring, Theory of the thermoelectric power of semiconductors, *Phys. Rev.* **96**, 1163 (1954).
- [66] Y. G. Gurevich and O. L. Mashkevich, The electron-phonon drag and transport phenomena in semiconductors, *Phys. Rep.* **181**, 327 (1989).